Received: 9 February 2026 | Revised: 24 April 2026 | Accepted: 7 May 2026

DOI: 10.1002/cjce.70472

RESEARCH ARTICLE

THE CANADIAN JOURNAL OF CHEMICAL ENGINEERING

Bituminous membrane design for radon protection

Carmen Manteca-Martínez[1] | **Ángel Yedra Martínez**[1] | **Lucía Pérez-Gandarillas**[1] | **Daniel Rábago**[2] | **Carlos Sainz**[2] | **Germán Ibáñez**[3] | **Luis Rodríguez-Guadarrama**[3]

[1]CTC Technology Centre, Scientific and Technological Park of Cantabria (PCTCAN), Santander, Spain

[2]Laboratory of Environmental Radioactivity (LaRUC), University of Cantabria, Santander, Spain

[3]Dynasol Elastomers SAU, Gajano, Spain

Correspondence
Luis Rodríguez-Guadarrama, Dynasol Elastomers SAU, Gajano 39792, Spain.
Email: larodriguezgua@repsol.com

Funding information
INNOVA CANTABRIA, Grant/Award Number: 2021/INN/36

Abstract

Radon gas is considered a significant hazard to human health due to its radioactive character and its relationship with lung cancer. In response, national and international organizations have developed regulations to reduce radon exposure in indoor environments. In this study, novel nanocomposites based on styrene–butadiene–styrene (SBS) copolymers and bitumen were developed by incorporating two-dimensional (2D) nanomaterials to create effective physical barriers against radon gas. The resulting materials were evaluated for potential application in the building sector to mitigate radon permeation. The best-performing formulations achieved radon diffusion coefficients on the order of 10^{-12} m^2/s, below the limit established by European Directive 2013/59/EURATOM for radon barrier materials. Mechanical and physical characterization confirmed that the incorporation of nanofillers did not significantly alter the properties of the SBS–bitumen matrix. Overall, the developed nanocomposites exhibit promising performance as functional barrier materials for reducing indoor radon exposure and improving building health safety.

KEYWORDS

graphene, nanoparticles, radon, radon barrier materials, radon mitigation

1 | INTRODUCTION

Radon (^{222}Rn) is a naturally occurring radioactive gas generated from the decay of radium (^{226}Ra), commonly present in granitic soils. Due to its gaseous nature, radon can migrate through porous media and enter buildings through cracks, joints, and other discontinuities, accumulating in poorly ventilated indoor environments. Long-term exposure to elevated radon concentrations is associated with an increased risk of lung cancer, and radon is currently recognized as the second leading cause of lung cancer overall and the primary cause among non-smokers.[1–5]

In response to these health risks, regulatory frameworks have been established to limit indoor radon exposure. In Europe, Directive 2013/59/EURATOM requires Member States to define national reference levels and implement mitigation strategies.[6] In Spain, this Directive has been partially transposed into national legislation through the Technical Building Code (CTE), which establishes a reference level of 300 Bq/m^3 for indoor environments and recommends the use of radon barriers with diffusion coefficients below 10^{-11} m^2/s and a minimum thickness of 2 mm.[6–8]

Mitigation strategies for radon ingress in buildings include soil depressurization systems, sealing of entry pathways, and the use of barrier materials. Among these, passive barrier systems are particularly attractive due to their ease of implementation in both new construction and retrofitting applications. However, the development

of materials with sufficiently low radon permeability remains a challenge.

Recent research on radon barriers has primarily focused on the evaluation of commercial materials and the development of measurement methodologies for radon diffusion coefficients.[9–11] Although some coating systems have demonstrated high efficiency in reducing radon levels,[12] the design of advanced materials specifically tailored to limit radon transport remains limited. In particular, the application of nanocomposite materials for radon barrier purposes has not been extensively explored.

In the field of polymer nanocomposites, the incorporation of two-dimensional (2D) nanomaterials such as clays and graphene nanoplatelets has been widely reported to improve gas barrier properties. These improvements are generally attributed to the high aspect ratio of the fillers, which increases the tortuosity of diffusion pathways within the matrix. In addition, other mechanisms may contribute to gas transport reduction, including reversible physisorption on the surface of nanomaterials and changes in gas solubility within the composite system. The relative contribution of these mechanisms depends on factors such as filler type, dispersion, orientation, and concentration.[13–25]

Styrene–butadiene–styrene (SBS) copolymers are commonly used in bitumen modification for waterproofing membranes due to their flexibility and mechanical performance. The combination of SBS and bitumen provides a suitable matrix for the development of barrier materials with enhanced functional properties.

In this work, novel nanocomposite materials based on SBS and bitumen matrices incorporating 2D nanomaterials (clays and graphene nanoplatelets) have been developed as radon barriers for building applications. Advanced dispersion techniques, including three-roll milling, were employed to ensure adequate nanofiller distribution. The resulting materials were comprehensively characterized, with particular emphasis on radon diffusion behaviour, as well as mechanical, thermal, and physical properties.

2 | MATERIALS AND METHODS

Graphene nanoplatelets Av-PLAT-40 was purchased from Avanzare Innovación Tecnológica S.L. and graphene platelets CP-0081-HP were purchased from IoLiTec Ionic Liquids Technologies GmbH. Clay Cloisite 20A and BYK-MAX CT 4260 were purchased from BYK-Chemie GmbH. The properties of the nanofillers are reported in Table 1. Brugues S.A. was the supplier of cyclohexane. Nynas supplied Nyflex 223, a naphthenic oil with a kinematic viscosity of 0.88 cm^2/s. Calprene 411 (C411) is a 70/30 radial butadiene/styrene block copolymer from Dynasol Elastomers. Bitumen with penetration 160/220 from Repsol is a soft bitumen commonly used in the roofing market, alongside hard bitumen 70/100 from Repsol. The bitumen penetration grade indicates the range of penetration, expressed in tenths of a millimetre (dmm), of a standard needle under standardized conditions at 25°C. The availability of soft bitumens may decline in the forthcoming years, which could necessitate its substitution with harder bitumens.

Three mixing strategies were implemented to develop new nanocomposites. The first mixing strategy (E1) involved dispersing nanomaterials into C411. In this approach, formulations were prepared by combining the selected nanomaterials (graphene G1 or G2 and clay Ar1 or Ar2) and dispersing them using the three-roll milling technique. First, 100 g of C411 was dissolved in 1 L of cyclohexane under magnetic stirring for 1 h. Once dissolved, the graphene and clay were added to the mixture and manually stirred for 5 min. This mixture was then processed using the three-roll mill technique to ensure uniform dispersion. The gap between the rolls ranged from 120 μm (first pass) to 5 μm (final passes) with an apron roll speed of 300 rpm. After 40 min, the dispersed product was collected, and the cyclohexane was allowed to evaporate over several days to obtain a solid mixture for characterization testing. Subsequently, the samples were evaluated through radon diffusion tests, mechanical testing, colorimetry, and thermal conductivity measurements. Figure 1 presents a schematic diagram depicting

TABLE 1 Properties of the nanomaterials used.

2D Nanomaterials				
Nomenclature	**Commercial name**	**Thickness (nm)**	**Specific surface (m^2/g)**	**Lateral size (μm)**
G1	Graphene platelets CP-0081-HP	2	750	1–2
G2	Graphene nanoplatelets Av-PLAT-40	10	28	40
		Bulk density (kg/m^3)		**Particle size D50 (μm)**
Ar1	Clay Cloisite 20A	350		<10
Ar2	BYK-MAX CT 4260	400–600		<20

the mixing process used to obtain the E1 samples: M1–M4.

Following the completion of characterization tests, the sample exhibiting the lowest radon diffusion coefficient was chosen for implementation in strategies 2 and 3.

In strategy 2 (E2), nanofillers are mixed into bitumen heated to 180°C. The hot bitumen is manually stirred with the nanofillers, then blended with C411. The procedure for mixing C411, both with and without nanofiller, with bitumen is as follows: first, place the bitumen in an oven set at 180°C to bring it to the required temperature. Subsequently, the bitumen sample should be placed on a hot plate within a cabinet equipped with an extraction system. Insert a temperature probe into the bitumen and activate the Silverson Mixer®. Once the bitumen's temperature exceeds 170°C, incorporate C411. Maintain the mixing temperature at 180 ± 5°C with a rotational speed of 3500–4000 rpm. After blending for 50 min, distribute the bituminous blend into various instruments for final tests. Final tests include softening point temperature, penetration tests at 25°C, dynamic viscosity, and conducting cold bending tests. Figure 2 presents a schematic diagram depicting the mixing process used to obtain the E2 sample: M5.

In strategy 3 (E3), the nanofillers are incorporated into the oil using the three-roll milling technique to achieve uniform dispersion. Once we have the bitumen heated at 170°C, C-411 is incorporated into the bitumen with a high shear mixer and when the product is properly blended, we add the oil with nanofillers to the sample. The samples are subsequently prepared for characterization tests. Figure 3 presents a schematic diagram depicting the mixing process used to obtain the E3 sample: M6.

Table 2 presents the formulation matrix. Strategy 1 (E1) incorporated C411, graphene, and clays in samples M1 through M4. Strategy 2 (E2) produced sample M5 using these nanomaterials with bitumen and C411. Sample M6 was produced according to Strategy 3 (E3), which uses nanomaterials, oil, bitumen, and C411.

The radon diffusion coefficient[26] was determined using the method described in ISO/DTS 11665-13.[27]

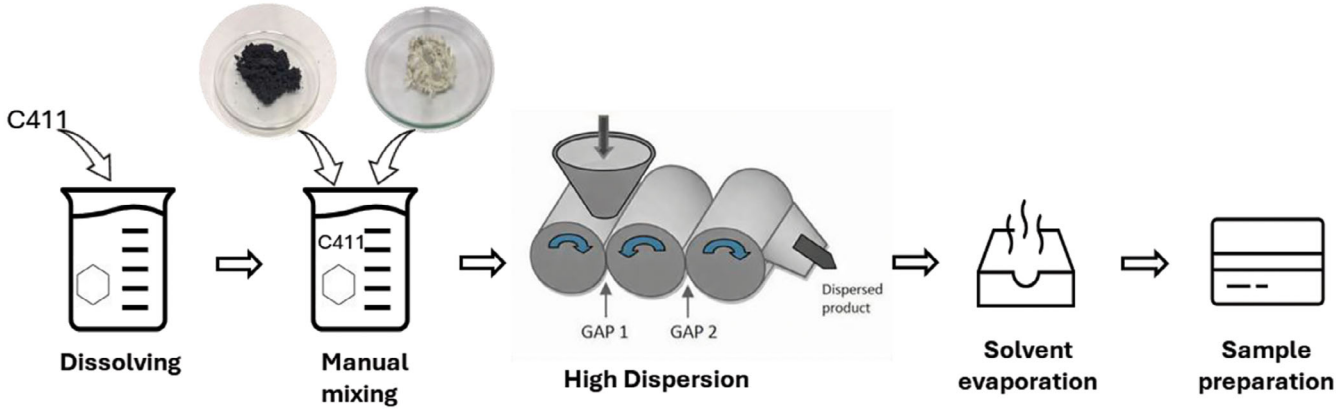

FIGURE 1 Schematic illustration of first mixing strategy (E1) samples preparation.

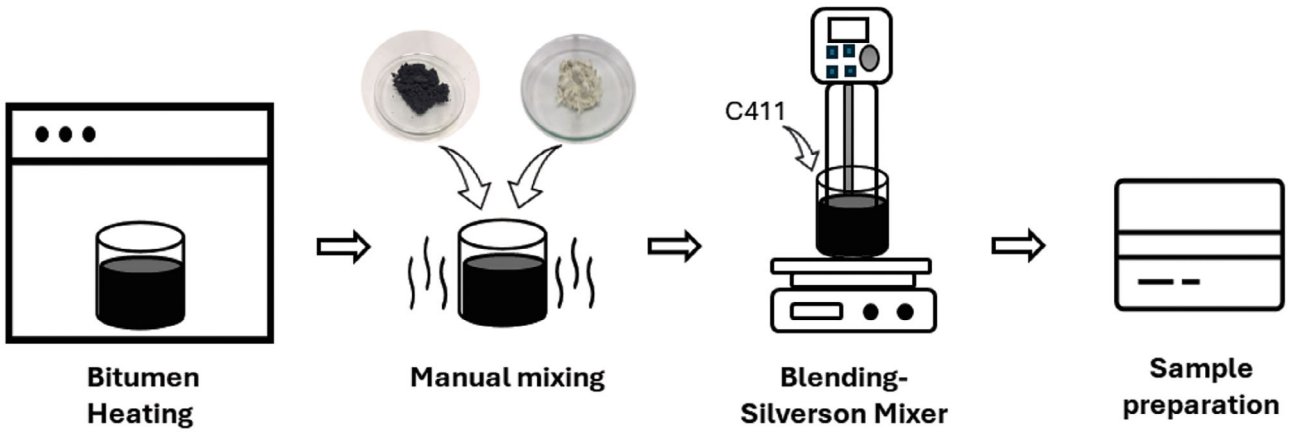

FIGURE 2 Illustration showing the preparation of strategy 2 (E2) samples.

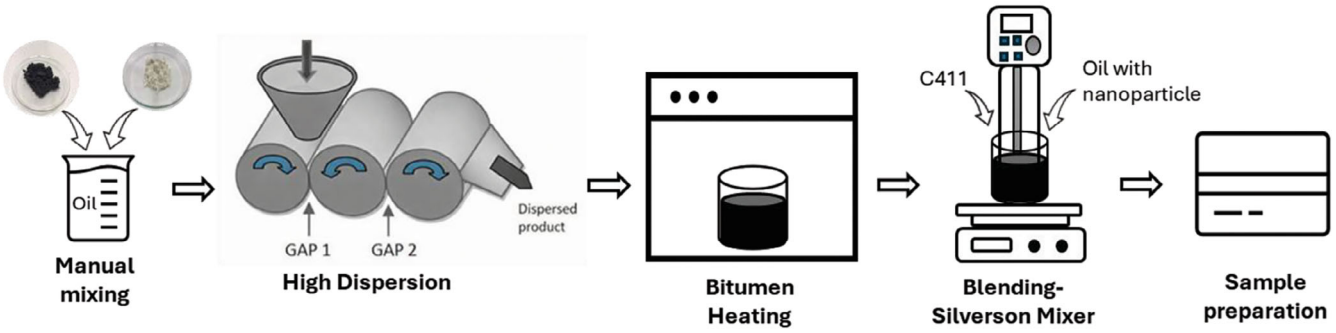

FIGURE 3 Schematic representation of the procedure for preparing strategy 3 (E3) samples.

TABLE 2 Matrix formulation of mixtures.

Component (wt.%)	E1 control	M1	M2	M3	M4	E2 control	M5	E3 control	M6
C411	100	84	84	84	84	10	9.8	10	9.8
Bitumen 160/220	-	-	-	-	-	90	87.9	-	-
Bitumen 70/100	-	-	-	-	-	-	-	85.9	84
Naphtenic oil	-	-	-	-	-	-	-	4.1	4.0
Ar1	-	15	-	15	-	-	-	-	-
Ar2	-	-	15	-	15	-	2.2	-	2.1
G1	-	1.0	1.0	-	-	-	-	-	-
G2	-	-	-	1.0	1.0	-	0.1	-	0.1

This method consists of positioning the sample specimen between two airtight chambers, referred to as the "source" and "receiver" containers. Radon concentrations on both sides of the sample are continuously monitored with two radon monitors. The radon diffusion coefficient D (m^2/s) is obtained by solving Fick's second law for one-dimensional transient diffusion through a plane membrane, which accounts for radioactive disintegration during transport:

$$\frac{\partial C(x,t)}{\partial t} = D \cdot \frac{\partial^2 C(x,t)}{\partial x^2} - \lambda \cdot C(x,t) \quad (1)$$

where C (x, t) the radon concentration within the sample (Bq/m^3), x the distance from the surface exposed to radon (m), λ the radon decay constant (s^{-1}) and t the time (s). Boundary conditions are defined by the radon concentrations measured in the source and receiver chambers. The numerical solution, implemented through the IterRn software, iteratively determines the value of D that best fits the experimentally measured temporal evolution of radon concentration in the receiver chamber.[28]

The experimental set up consists of two cubic chambers with an inner volume 25,672 cm^3 (29.5 cm geometrical side), and the sample to be tested must have a square surface of 784 cm^2 (28 cm geometrical side) which is adhered and sealed with acrylic putty on the top of the source container. The thickness of the sample is measured at least in four points with a calliper. The radon source used in the source container is natural soil with a high 226Ra content confined in a radon diffusive 125 mL plastic container. The availability of several sources with different 226Ra allows to reach radon concentrations in the source container of the order of MBq/m^3.[26]

The measuring devices are radon monitors of the Radon Scout type (SARAD, Germany), periodically calibrated in the ISO/IEC 17025 accredited radon chamber available at LaRUC, and placed on each container to minimize randon leakage from the experimental setup schematically illustrated in Figure 4.

The data acquisition method aligns with 'Method C' as outlined in the ISO reference standard. To achieve a steady state in the concentration profile within the material's thickness, the source and radon monitor are placed in the source container with the sample positioned on top. After 10 days, the receiver container is added, followed by a measurement period of another 10 days.

The IterRn (Version 2016) is a specific software developed by Zbynek Svoboda and Martin Jiranek (Czech Technical University in Prague, Czech Republic) and it is used for the calculation of the diffusion coefficient. The software computes the temporal evolution of the radon

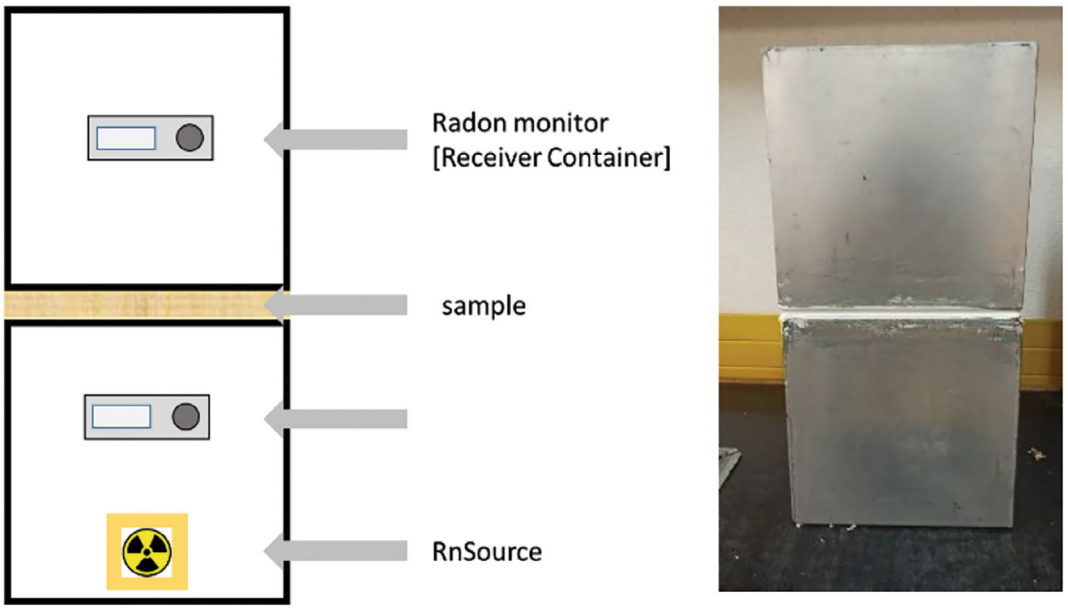

FIGURE 4 Schematic and photography of the experimental setup.

exhalation rate from the analyzed sample, as well as the radon concentration within the receiver chamber. Through an iterative numerical process, the radon diffusion coefficient is subsequently determined, as illustrated in Figure 5.[29]

A C-Therm TCi thermal conductivity analyzer,[30] employing the modified transient plane source (MTPS) technique, was used to determine the thermal conductivity and effusivity of the samples. The device utilizes a one-sided, interfacial heat reflectance sensor that applies a brief, constant heat input to the sample. Both thermal conductivity and effusivity are measured directly and rapidly, providing a comprehensive characterization of the thermal properties of the material. Figure 6 illustrates the types of samples used for these measurements.

After preparing test samples with 2 mm thickness and 6 mm width, we use a dynamometer to evaluate them. This equipment calculates the following properties:

Tensile strength is the amount of force required to stretch a test sample to the point of failure. This test is performed placing a dumbbell shaped part into the grips of a dynamometer. The dynamometer pulls the grips apart steadily until the dumbbell breaks. The force at rupture is known as ultimate tensile strength.

Strain is measured by stretching the sample same as above and measuring the change in length from original. Strain is expressed as a percentage of the original length. Ultimate strain is the percentage change in length from original to rupture.

Modulus is the force at a specific strain, such as 100%, 200%, or 300%. Modulus is utilized for comparison purposes at different strain levels, such as 100% strain, which is referred to as 'M100'.

The softening point specifies bitumen properties at high service temperatures and represents a conventional, approximate upper limit of the viscoelastic consistency. The test involves determination of the conventional temperature at which bitumen acquires a specific consistency. Bitumen softening point testing is usually performed by the ring and ball method (R&B in short). Two bitumen samples placed in metal rings are heated in controlled manner in a liquid (glycerin for R&B higher than 80°C), placed in a glass beaker, with each bitumen-filled ring supporting a steel ball. The softening point is indeed the average temperature at which both bitumen rings soften to the extent that each ball, covered in bitumen, travels 25.0 mm ± 0.4 mm. The R&B softening point test is performed according to PN-EN 1427: *Bitumen and bituminous binders. Determination of the softening point*.

The primary method for bitumen classification in the European standardization framework is the penetration test at 25°C. The test involves determination of bitumen consistency expressed as the distance that a standardized steel needle penetrates vertically into a bitumen sample at a specific temperature. The needle load is 100 g, and

the loading time equals 5 s. The penetration unit is 0.1 mm, which corresponds to the needle penetration depth in the bitumen sample.

The interpretation of penetration test results is straightforward: for instance, bitumen with a penetration of 200 dmm is softer than bitumen with a penetration of 100 dmm because the needle penetration depth is 20 mm in the former case, compared to 10 mm in the latter. Generally, greater penetration indicates softer bitumen. The test can be performed at different temperatures; however, 25°C is typically used for bitumen classification purposes. The penetration test is conducted according to PN-EN 1426: *Bitumen and bituminous binders-Determination of needle penetration*.

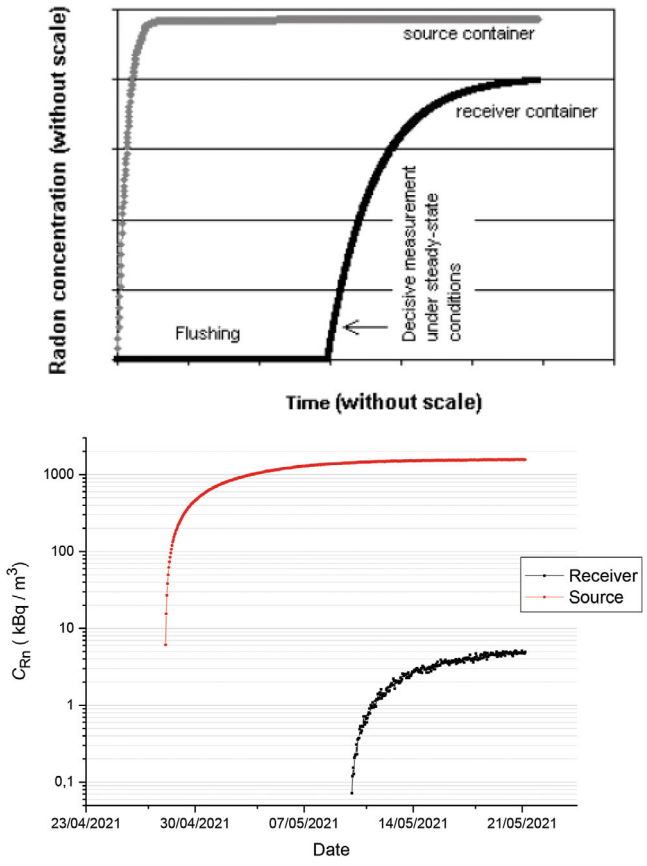

FIGURE 5 Typical shape of data obtained following method C of ISO/TS 11665-13: 2017.

Viscosity testing can be performed using different methods and instruments, and at various temperatures. For highly modified bitumen, viscosity testing is typically conducted at 180°C, using a Brookfield rotary viscometer to measure dynamic viscosity. Dynamic viscosity testing is conducted according to PN-EN 13302: *Bitumen and bituminous binders. Determination of dynamic viscosity of bituminous binder using a rotating spindle apparatus*. Brookfield dynamic viscosity testing applies the difference in the resistance of a rotating spindle immersed in bitumen with different viscosity. Resistance increases as bitumen viscosity increases, while the spindle's torque remains within the appropriate pre-set range. Dynamic viscosity testing involves the determination of the relationship between relative resistance to the rotation of the spindle in a special container holding the tested sample at the pre-set spindle rotational speed. Dynamic viscosity of the tested liquid is read out directly on the viscometer, whose spindle torque must be within a specific range. If the condition is not met, the spindle is replaced with another one, having a different shape coefficient.

Through compression moulding at high temperature, sheets of bituminous membranes are produced from which test specimens measuring 170 × 25 mm are cut. In the cold bending test apparatus, five test specimens are placed around a cylindrical bending mandrel, and the elevation system is connected. The test begins at −10°C, with the temperature being decreased by 2° incrementally. At each temperature level, the test specimens are folded 180°

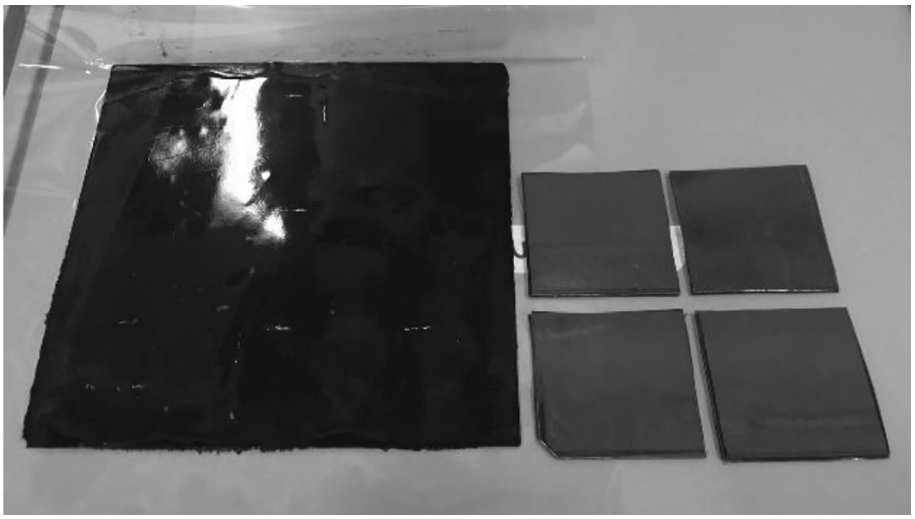

FIGURE 6 Sample examples for diffusion and thermal conductivity tests.

around the central mandrel. The cold bending temperature of the bituminous membrane is identified when three test specimens crack or fracture.

Waterproofing sheets or roofing sheets are typically tested for water penetration resistance, vapour durability, or moisture resistance. The samples are exposed to high humidity conditions for an extended period to determine whether these conditions affect the mechanical and physical properties of the formulations. The test involves exposing the samples for 1 month at a temperature of 23 ± 1°C and relative humidity of 75% ± 2% in an environmental chamber. Figure 7 shows an image of the test.

3 | RESULTS AND DISCUSSION

Table 3 shows the results of the tensile test performed on the nano-additivated C411 samples prepared in strategy E1. Sample M1 shows the highest values of breaking strength and modulus, as well as the lowest elongation. This was attributed to the very high aspect ratio of the graphene filler[31] and the high distribution of graphene layers in the polymer matrix as well as interfacial bonding between the graphene layers and polymer matrix.[32]

FIGURE 7 Samples in the environmental chamber during the degradation test.

Samples M2 to M4 display comparable values for these parameters.

Table 4 shows the thermal conductivity and effusivity of mixtures using strategy E1. The values for nanocomposites do not vary significantly with different fillers. Samples M1–M4 have uniform thermal conductivity.

Table 5 presents the radon diffusion coefficient results for E1 samples, including the measurement uncertainty and the improvement relative to the E1 control. The prepared films measured 280 × 280 mm, and one film per sample was tested.

The results for strategy E1 show that the addition of nanofillers reduces the diffusivity of radon gas through the matrix of C411. Samples M1 and M4 exhibit the lowest diffusion coefficients, with reductions of 77% and 80%, respectively. This behaviour is primarily attributed to the high aspect ratio of the nanoclay and graphene nanoplatelets, which increases the tortuosity of the diffusion pathways within the polymer matrix.[22,23,33] However, additional mechanisms may also contribute to the observed reduction in radon transport. Reversible physisorption of radon on nanofiller surfaces and changes in gas solubility within the composite matrix may occur. The impact of these mechanisms likely depends on nanofiller dispersion and their interaction with the polymer matrix. The nanomaterials used in M4 were BYK MAX CT4260 clay and av-PLAT-40 graphene. These nanofillers were also utilized to prepare samples M5 and M6 for strategies E2 and E3, respectively.

The results of the tensile test, conducted following the environmental degradation test, are compiled and shown in Table 6.

The mechanical properties observed after environmental aging indicate a reduction in elongation and breaking strength, alongside an increase in elastic modulus across all samples. This outcome suggests that the samples exhibit increased stiffness and diminished elasticity. This phenomenon is likely due to crosslinking reactions taking place within C411.

Table 7 presents the results of tests conducted on samples with C411/bitumen prepared using strategy E2 or E3. The data indicates that the softening point R&B

TABLE 3 Tensile test results for E1 mixtures.

Sample	Strain (%)	Breaking strength (MPa)	Elastic modulus 100 (MPa)	Elastic modulus 300 (MPa)	Elastic modulus 500 (MPa)
M1	800	31.5	5.0	7.0	10.4
M2	840	26.3	4.0	5.7	8.4
M3	850	25.2	4.1	5.5	7.8
M4	890	23.7	4.1	5.3	7.2

remains constant in the samples, unaffected by the addition of nanofillers, which is a crucial parameter for the final application. Regarding cold bendability, it also remains stable, while penetration at 25°C decreases slightly with the inclusion of nanofillers, indicating a slight increase in hardness of the sheet. This improvement is advantageous for the application, considering the consistency in cold bendability.

Following the environmental degradation test, the physical properties of the nano-additivated bitumen samples are presented in Table 8.

Figure 8 compares bitumen samples before and after aging, showing changes in softening point, penetration, and dynamic viscosity.

Figure 8 shows that samples exposed to 75% relative humidity for a month exhibit change in their properties. For soft bitumen 160/220, which corresponds to samples E2 control and M5, the softening point remains nearly unchanged, with a slight increase (1%) for the sample with nanoparticles (M5) compared to its undegraded sample. Penetration measurements decrease for both mixtures, indicating that the samples become stiffer or harder after exposure to humidity. Viscosity measurements show an increase, more pronounced for the sample with nanoparticles. This is due to the high dispersion of the nanoparticles in the polymer matrix by the three-roll mill process, which breaks up agglomerates and distributes individual nanoparticles in the polymer, thereby increasing the mixture's viscosity. This effect was observed in previous studies.[33]

For hard bitumen 70/100, corresponding to sample E3 control and M6, the softening point decreased by approximately 5% for the sample containing nanoparticles (M6) compared to the sample without degraded nanoparticles. For the reference sample (E3 control), measurements were not obtainable. Regarding penetration measurements, both mixtures showed a decrease in value, with the reference sample exhibiting a more significant reduction. The viscosity of the E3 control sample increased significantly from 1810 to 4775 cP. The lower viscosity in M6 can be attributed to the shielding (barrier) effect of graphene platelets, which can hinder oxygen transport and thereby slow down thermo-oxidative aging,

TABLE 4 Thermal conductivity and effusivity results of M1–M4 samples.

Sample	Thermal conductivity (W/m·K)	Thermal effusivity ($Ws^{½}/m^2K$)
M1	0.23	574
M2	0.23	571
M3	0.22	559
M4	0.22	562

TABLE 5 Radon diffusion coefficient measurements of the E1 samples.

Sample	D (m^2/s) × 10^{-11}	Uncertainty (m^2/s) × 10^{-11}	Reduction (%)
E1 Control	9.2	2.6	-
M1	2.1	0.6	77
M2	2.6	0.7	72
M3	2.4	0.7	74
M4	1.8	0.5	80

TABLE 6 Tensile test results of E1 samples after aging.

Sample	Strain (%)	Breaking strength (MPa)	Elastic modulus 100 (MPa)	Elastic modulus 300 (MPa)	Elastic modulus 500 (MPa)
M1	610	26.6	6.3	11.7	19.5
M2	590	24.5	6.2	11.6	19.1
M3	550	21.3	6.2	11.1	18.8
M4	560	21.8	6.3	11.2	18.6

TABLE 7 Results of physical tests on unaged bitumen for E2 and E3 samples.

Sample	Softening Point R&B (°C)	Penetration at 25°C (dmm)	Dynamic viscosity (cP)	Cold bending test (°C)
E2 control	113	51	1650	−30
M5	112	42	1850	−28
E3 control	116	50	1810	−32
M6	117	46	1460	−28

TABLE 8 Physical test results for aged bitumen samples E2 and E3.

Sample	Softening Point R&B (°C)	Penetration at 25°C (dmm)	Dynamic viscosity (cP)
E2 Control	112	41	2166
M5	113	39	2590
E3 Control	N/A	40	4775
M6	110	42	1692

as reported by Yang et al.[34] In our study, this interpretation is supported indirectly by the smaller viscosity increase observed for the graphene-containing sample (M6) after the environmental degradation test, compared with the E3 control under the same conditions.

Both modified bitumens with C411 become harder after high humidity exposure, with a slight change in softening point. However, variations are less pronounced when nanoparticles are used, suggesting that plate-like nanofillers may contribute to aging resistance mainly through a physical shielding (gas-barrier) effect that reduces oxygen diffusion into the binder. In addition, graphene-based fillers have been reported to exhibit radical-scavenging (antioxidant) behaviour; however, this contribution was not directly assessed in the present work.

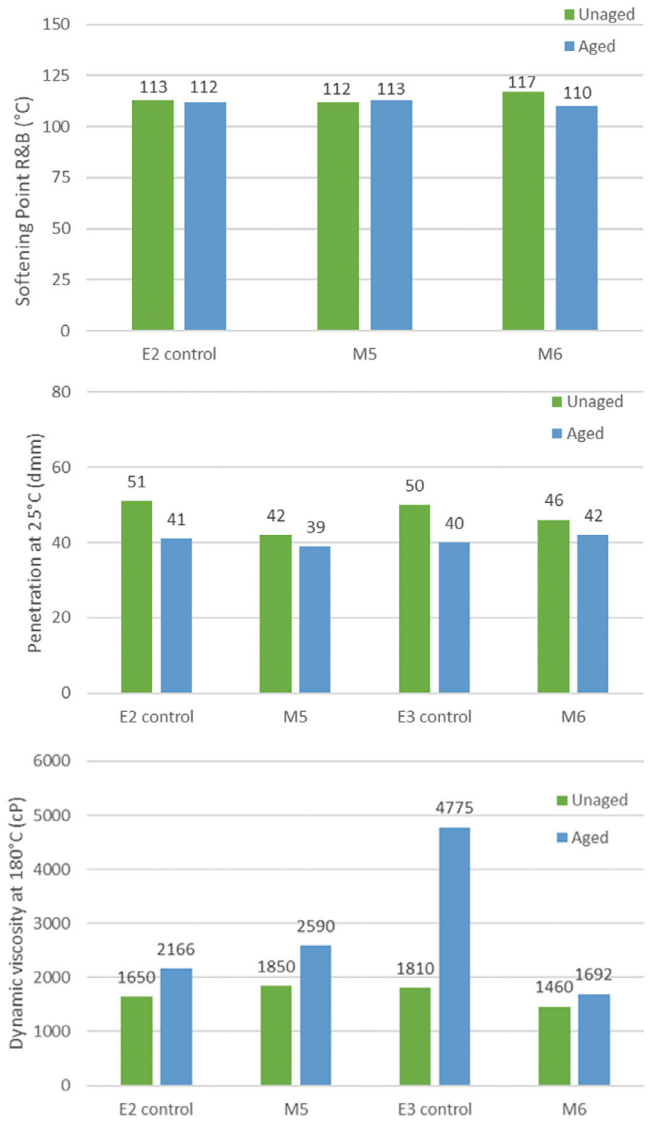

FIGURE 8 Comparison of the softening point of bitumen samples before and after environmental degradation test: Softening point, penetration, and dynamic viscosity.

Table 9 presents radon diffusion coefficients for mixtures E2 and E3, categorized by mixing strategies. It includes diffusion coefficients, measurement uncertainties, and improvements compared to control samples. The tests involved one 280 × 280 mm film per sample.

In strategy E2, both E2 Control and M5 samples show a low diffusion coefficient. The inclusion of nanofillers (M5) results in a 29% reduction in the diffusion coefficient. Although the nanofiller content is relatively low, an improvement in barrier performance is observed. This behaviour is mainly associated with the homogeneous dispersion of high-aspect-ratio fillers, which promotes the development of tortuous diffusion pathways.[31,35]

Nevertheless, other contributions, such as reversible physisorption on the nanofiller surface and modifications in radon solubility within the matrix, may also play a role. Due to the limitations of the present study, these effects could not be independently quantified.

In strategy E3, the incorporation of oil slightly reduces the effective nanofiller content in mixture M6, and no improvement in the radon diffusion coefficient is observed relative to the control sample. This behaviour may be associated with a nanofiller concentration below the threshold required to generate a significant barrier effect, as well as potential changes in filler dispersion or matrix–filler interactions.

Overall, the reduction in radon diffusion observed in the developed nanocomposites is attributed to a combination of mechanisms, including increased tortuosity of diffusion pathways, potential reversible physisorption on nanofiller surfaces, and possible changes in gas solubility within the matrix. Further studies would be required to decouple and quantify the individual contribution of each mechanism.

According to the Spanish Technical Building Code (CTE), an acceptable barrier is a foil-type barrier with a radon diffusion coefficient of less than 10^{-11} m^2/s and a minimum thickness of 2 mm. Both samples M5 and M6, along with their references, E2 control and E3 control, meet this requirement.

TABLE 9 Radon diffusion coefficient results of E2 and E3 samples.

Strategy	Sample	D (m^2/s) × 10^{-12}	Uncertainty (m^2/s) × 10^{-12}	Reduction (%)
E2	E2 Control	7.0	2.0	-
	M5	5.0	1.4	29
E3	E3 Control	4.0	1.1	-
	M6	6.6	1.8	−65

4 | CONCLUSIONS

The radon gas barrier properties of various polymer- and bitumen-based nanocomposite formulations were evaluated to study the effect of nanofillers on gas permeability. The results indicate that the incorporation of two-dimensional nanomaterials, such as clay and graphene nanoplatelets, effectively reduces radon diffusion, mainly due to the increased tortuosity of diffusion pathways induced by their high aspect ratio.

In addition to tortuosity effects, other mechanisms such as reversible physisorption on nanofiller surfaces and possible changes in gas solubility within the matrix may also contribute to the observed behaviour, although their individual contributions could not be quantified in the present study.

In the case of polymer-based formulations, C411 matrix exhibited the lowest radon diffusion coefficient when loaded with 15 wt.% of BYK-MAX CT 4260 and 1 wt.% of graphene nanoplatelets Av-PLAT-40, achieving a value of 1.8×10^{-11} m^2/s. This demonstrates the synergistic effect of combining organoclay and graphene-based nanofillers to restrict radon transport through the polymer matrix. Mechanical and thermal analyses indicated that these nanocomposites exhibited high tensile strength and elastic modulus values, coupled with reduced elongation. After environmental aging, all polymer-based samples showed a decrease in elongation and tensile strength, along with an increase in elastic modulus, suggesting increased stiffness and reduced elasticity.

For bitumen-based formulations, the lowest radon diffusion coefficients were obtained in Bitumen 160/220 combined with C411, 2.2 wt.% BYK-MAX CT 4260, and 0.1 wt.% graphene nanoplatelets Av-PLAT-40, reaching a value of 5.0×10^{-12} m^2/s, as well as in Bitumen 70/100 with C411 and oil without nanomaterials, showing a similar diffusion coefficient of 4×10^{-12} m^2/s. These results suggest that nanomaterial incorporation can significantly improve the radon barrier properties of bituminous matrices, although certain formulations may inherently offer low permeability even without nanofillers. Physical properties were conducted to evaluate the overall impact of nanofillers on nanocomposite performance. The inclusion of nanofillers led to only minor changes in these properties, indicating that the final mechanical and thermal behaviour of the developed films remain largely unaffected. Environmental degradation analysis showed increased hardness in all bitumen-based mixtures after exposure to high humidity conditions, with slight variations in ring-ball softening temperatures. These changes were less significant for the mixtures containing nanoparticles, which is consistent with a physical shielding (oxygen-barrier) contribution of plate-like nanofillers that can slow down thermo-oxidative aging by reducing oxygen transport through the binder.

In summary, using high-aspect-ratio nanofillers represents a promising strategy for the development of effective radon barrier materials that meet the requirements established by the CTE.

AUTHOR CONTRIBUTIONS

Carmen Manteca-Martínez: Investigation; writing – original draft; supervision. **Ángel Yedra Martínez:** Conceptualization; investigation; supervision. **Lucía Pérez-Gandarillas:** Conceptualization; investigation. **Daniel Rábago:** Conceptualization; investigation. **Carlos Sainz:** Conceptualization; investigation. **Germán Ibáñez:** Conceptualization; investigation; supervision. **Luis Rodríguez-Guadarrama:** Investigation; writing – original draft.

ACKNOWLEDGEMENTS

The authors gratefully acknowledge the financial support provided by FEDER and The Government of Cantabria (Spain) for project 2021/INN/36 under the INNOVA CANTABRIA 2022 program. During the preparation of this work, the author(s) used ChatGPT to assist with grammar checking and rephrasing to enhance the readability of the manuscript. The author(s) reviewed and edited the content as necessary and take full responsibility for the final version of the published article.

PEER REVIEW

For transparency, the peer review documents associated with this article are available at https://doi.org/10.1002/cjce.70472.

DATA AVAILABILITY STATEMENT

The data that support the findings of this study are available upon request from the corresponding author. The data are not publicly available due to privacy or ethical restrictions.

ORCID

Carmen Manteca-Martínez https://orcid.org/0000-0002-8619-8155
Ángel Yedra Martínez https://orcid.org/0000-0002-9387-7332
Daniel Rábago https://orcid.org/0000-0002-2285-8767
Carlos Sainz https://orcid.org/0000-0003-2029-4512
Luis Rodríguez-Guadarrama https://orcid.org/0000-0002-3699-5957

REFERENCES

[1] World Health Organization. https://www.who.int/ (accessed: December 2025).
[2] D. S. Ting, *Int. J. Environ. Stud.* **2010**, *67*, 100.

[3] IARC, *Monographs on the Evaluation of the Carcinogenic Risks to Humans. Man-Made Mineral Fibers and Radon*, WHO IARC Publications, Lyon, France **1988**.
[4] A. C. Syuryavin, S. Park, M. M. Nirwono, S. H. Lee, *Nucl. Eng. Technol.* **2020**, *52*, 2370.
[5] An official website of the European Union, Access to European Union Law. https://eur-lex.europa.eu/ (accessed: December 2025).
[6] Spanish Ministry for Transport, Mobility and the Urban Agenda, *Basic Document DB-HS on Health and Safety. Section 6-Protection Against Radon*, *Technical Building Code (CTE)*, Government of Spain, Madrid, Spain **2019**. https://www.codigotecnico.org (accesed: December 2025).
[7] Ministry of Social Affairs and Health, *National Radon Action Plan*, Ministry of Social Affairs and Health, Helsinki, Finland **2021**.
[8] B. Ruvira, B. García-Fayos, B. García-Gimeno, J. M. Arnal, G. Verdú, *Radiat. Phys. Chem.* **2024**, *223*, 111916.
[9] M. Jiránek, J. Hůlka, *Sci. Total Environ.* **2001**, *272*, 79.
[10] G. Keller, B. Hoffmann, T. Feigenspan, *Sci. Total Environ.* **2001**, *272*, 85.
[11] W. Z. Daoud, K. J. Renken, *Sci. Total Environ.* **2001**, *272*, 127.
[12] W. W. G. Gao, Y. H. Tang, C. M. Tam, X. F. Gao, *Atmos. Environ.* **2008**, *42*, 8634.
[13] F. Pacheco-Torgal, *Build. Environ.* **2012**, *58*, 270.
[14] B. Frutos Vázquez, *Doctoral Dissertation*, E.T.S. Arquitectura (UPM)(Seri Kembangan, Malaysia) **2009**.
[15] E. Espuche, *Polym. Test.* **2023**, *125*, 108124.
[16] A. Idris, A. Muntean, B. Mesic, *J. Coat. Technol. Res.* **2022**, *19*, 699.
[17] B. M. Yoo, H. J. Shin, H. W. Yoon, H. B. Park, *J. Appl. Polym. Sci.* **2014**, *131*, 39628.
[18] N. Baig, *Composites Part A Appl. Sci. Manuf.* **2023**, *165*, 107362.
[19] F. E. Z. Rahmaoui, P. Mederic, N. Aït Hocine, A. Aït Saada, N. Poirot, I. Belaidi, *Appl. Clay Sci.* **2017**, *150*, 244.
[20] B. S. Bouakaz, I. Pillin, A. Habi, Y. Grohens, *Appl. Clay Sci.* **2015**, *116*, 69.
[21] B. Tan, N. L. Thomas, *J. Membr. Sci.* **2016**, *514*, 595.
[22] Y. Zhang, Q. Liu, S. Zhang, Y. Zhang, H. Cheng, *Appl. Clay Sci.* **2015**, *111*, 37.
[23] Y. Cui, S. I. Kundalwal, S. Kumar, *Carbon* **2016**, *98*, 313.
[24] E. R. Sadiku, A. B. Reddy, D. Gnanasekarana, B. Oboirien, in *Nanostructured Polymer Blends for Gas/Vapor Barrier and Dielectric Applications* (Eds: S. Thomas, R. Shanks, S. Chandrasekharakurup), William Andrew Publishing, Norwich, NY **2016**, p. 239.
[25] Mangala Joshi, B. Adak, B. S. Butola, *Prog. Mater. Sci.* **2018**, *97*, 230.
[26] M. Jiranek, Z. Svoboda, *Build. Environ.* **2009**, *44*, 1318.
[27] International Organization for Standardization (ISO), *Measurement of Radioactivity in the Environment — Air: Radon-222 — Part 13: Indirect Measurement. ISO/TS 11665-13*, International Organization for Standardization, Geneva, Switzerland **2017**.
[28] M. Jiránek, K. Rovenská, *Appl. Radiat. Isot.* **2012**, *70*, 752.
[29] J.-J. Tejado-Ramos, A. Alvarez-Toral, J. Guillén, M. Carmona-Carmona, F. J. Muñoz-Almaraz, *Constr. Build. Mater.* **2024**, *414*, 134967.
[30] C-Therm Technologies. https://www.ctherm.com/ (accessed: December 2025).
[31] T. Kuilla, S. Bhadra, D. Yao, N. H. Kim, S. Bose, J. H. Lee, *Prog. Polym. Sci.* **2010**, *35*, 1350.
[32] S. Sinha Ray, M. Okamoto, *Prog. Polym. Sci.* **2003**, *28*, 1539.
[33] J. Njuguna, *Structural Nanocomposites, Perspectives for Future Applications*, Springer, Heidelberg, Germany **2013**.
[34] Q. Yang, Q. Zhu, R. Xu, L. Hao, G. Lu, D. Wang, *Langmuir* **2025**, *41*, 842.
[35] J. Wu, G. Huang, H. Li, S. Wu, Y. Liu, J. Zheng, *Polymer* **2013**, *54*, 1930.

How to cite this article: C. Manteca-Martínez, Á. Y. Martínez, L. Pérez-Gandarillas, D. Rábago, C. Sainz, G. Ibáñez, L. Rodríguez-Guadarrama, *Can. J. Chem. Eng.* **2026**, 1. https://doi.org/10.1002/cjce.70472